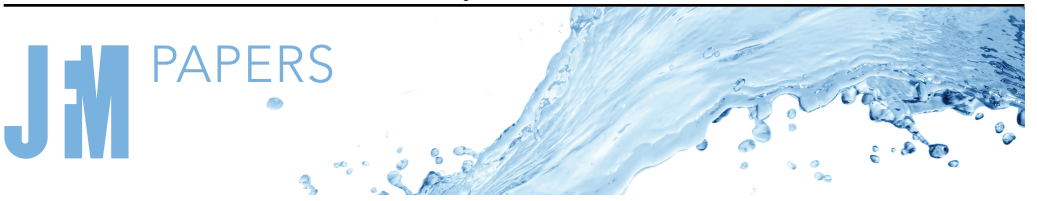
J. Fluid Mech. (2026), *vol.* 1034, A17, doi:10.1017/jfm.2026.11477



Reciprocal swimming in viscoelastic granular hydrogels

Hongyi Xiao[1,2,†], **Jing Wang**[3,†], **Achim Sack**[1], **Ralf Stannarius**[3,4] and **Thorsten Pöschel**[1]

[1]Institute for Multiscale Simulation, Friedrich-Alexander-Universität Erlangen-Nürnberg, Erlangen, Germany

[2]Department of Mechanical Engineering, University of Michigan, Ann Arbor, USA

[3]Institute of Physics, Otto von Guericke University Magdeburg, Magdeburg, Germany

[4]Department of Engineering, Brandenburg University of Applied Sciences, Brandenburg an der Havel, Germany

Corresponding authors: Hongyi Xiao, hongyix@umich.edu; Thorsten Pöschel, thorsten.poeschel@fau.de

(Received 18 October 2025; revised 27 February 2026; accepted 25 March 2026)

We experimentally study a scallop-like swimmer with reciprocally flapping wings in a nearly frictionless, cohesive granular medium consisting of hydrogel spheres. Significant locomotion is found when the swimmer's flapping frequency matches the inverse relaxation time of the material. Remarkably, the swimmer moves in the opposite direction compared with its motion in a cohesion-free granular material of hard plastic spheres. At higher or lower frequencies, we observe no motion of the swimmer, apart from a short initial transient phase. X-ray radiograms reveal that the wing motions create low-density zones, which in turn give rise to a hysteresis in drag and propulsion forces. This time-dependent effect, combined with the swimmer's inertia, accounts for locomotion at intermediate frequencies.

Key words: granular media, viscoelasticity, swimming/flying

1. Introduction

Locomotion in complex media, such as colloids, polymer solutions and granular materials, is characterised by the interaction of swimmers with nonlinear rheological properties and non-continuum effects (Arratia 2022). In polymeric liquids, swimmers like cells, bacteria

[†]The two authors contributed equally to this work.

© The Author(s), 2026. Published by Cambridge University Press. This is an Open Access article, distributed under the terms of the Creative Commons Attribution licence (https://creativecommons.org/licenses/by/4.0/), which permits unrestricted re-use, distribution and reproduction, provided the original article is properly cited.

https://doi.org/10.1017/jfm.2026.11477 Published online by Cambridge University Press

and micro-robots can take advantage of liquid properties including shear-rate-dependent viscosity (Fu, Wolgemuth & Powers 2009; Qiu *et al.* 2014; Riley & Lauga 2017; Han *et al.* 2020) and elasticity involving hoop stress and normal stress differences (Normand & Lauga 2008; Keim, Garcia & Arratia 2012; Pak *et al.* 2012; Binagia & Shaqfeh 2021; Rogowski *et al.* 2021; Datta *et al.* 2022; Kroo *et al.* 2022). Propulsion gaits that stretch polymers in shear flow, thereby reducing the local viscosity or inducing elasticity in the medium, can enhance swimming efficiency under these conditions (Fu, Shenoy & Powers 2010; Wróbel *et al.* 2016). These effects also enable propulsion schemes such as reciprocal swimming (Keim *et al.* 2012; Qiu *et al.* 2014; Han *et al.* 2020), that are otherwise not possible in Newtonian liquids (Purcell 1977; Lauga 2011).

For media with heterogeneous microstructures (Balin *et al.* 2017; Zhang, Li & Ardekani 2018), significant non-continuum effects emerge when the characteristic length scale of the swimmer is comparable to that of a medium's constituents. For instance, in dense polymer solutions, a nanometre-scale beating flagellum may locally stretch out polymer coils, creating a polymer-depleted channel (Martinez *et al.* 2014). This structural modification results in a significantly lowered propulsive force when the flagellum revisits the wake. While subtle at the nanoscale, such non-continuum effects may become more pronounced for locomotion in complex media with larger constituent particles, such as granular materials.

Locomotion in granular media is a particularly rich problem, with examples ranging from sandfish lizards that undulate through sand (Maladen *et al.* 2009; Goldman 2014), to worms that burrow in soil via peristalsis (Dorgan 2018), and southern sand octopuses that fluidise the substrate to alter the resistance of submerged sand (Montana, Finn & Norman 2015). These systems are challenging to understand because granular matter can behave either like a flowing liquid (Forterre & Pouliquen 2008; Xiao *et al.* 2017, 2018) or like a load-bearing solid (Majmudar *et al.* 2007; Bi *et al.* 2011), depending on the conditions. The solid-like behaviour can arise from a jamming transition, which can be induced by isotropic pressure or shear (Liu & Nagel 1998; Bi *et al.* 2011; Behringer & Chakraborty 2018), and has important implications for locomotion. For instance, particles ahead of an intruder in a static bed often remain jammed, effectively enlarging the penetrating object (Buchholtz & Pöschel 1998; Brzinski III *et al.* 2013; Müller *et al.* 2014; Kang *et al.* 2018; Harrington, Xiao & Durian 2020). At large stresses, collective particle rearrangements dissipate elastic energy, giving rise to elasto-plastic behaviour (Schall & van Hecke 2010; Xiao *et al.* 2020, 2023). Most studies on locomotion, therefore, model granular materials as elasto-plastic or perfectly plastic continua, for which reduced-order approaches such as resistive force theories are applicable (Askari & Kamrin 2016; Agarwal *et al.* 2021, 2023).

Granular materials containing highly deformable, cohesive or nearly frictionless particles can display pronounced viscoelasticity, as in food products, powders, cosmetics and crude oil. Their flow behaviour differs markedly from that of rigid model materials, such as dry glass or plastic beads and poppy seeds, which are typically used in laboratory studies. Granular hydrogels provide a particularly interesting cohesive model system because they combine very low friction coefficients (≈ 0.01) with high elastic deformability (elastic moduli $1 \ldots 100$ kPa) (Ashour *et al.* 2017; Shakya *et al.* 2024). Due to their high water content, liquid capillary bridges can form between hydrogel particles, inducing cohesive forces. These effects lead to distinct time-dependent behaviours in shear flows (Dijksman & Mullin 2022; Wang *et al.* 2022; Farmani *et al.* 2025) and silo discharge (Stannarius *et al.* 2019; Harth *et al.* 2020; Wang *et al.* 2023). Because granular hydrogels combine viscoelasticity, reminiscent of polymeric liquids, with reconfigurable heterogeneous packing, swimming in such media is of particular interest. Beyond fundamental physics, it may also be relevant for applications such as microrobots navigating among blood cells.

https://doi.org/10.1017/jfm.2026.11477 Published online by Cambridge University Press

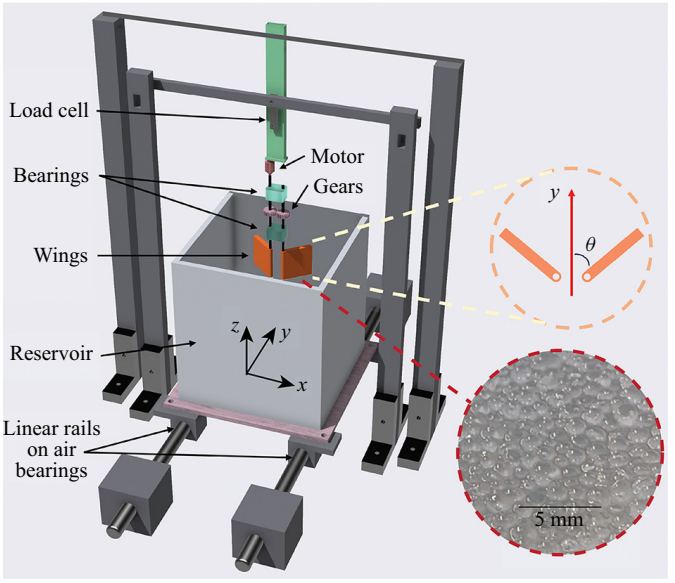


Figure 1. Experimental set-up for swimming in granular media. The apparatus consists of a pair of wings (15 mm × 15 mm × 1 mm) operating in a reservoir (70 mm × 70 mm × 85 mm) filled with granular particles. The inset shows a photograph of the hydrogel particles.

This study presents experiments with a scallop-inspired swimmer driven by two counter-rotating blades that flap reciprocally. The swimmer moves within a bed of hydrogel spheres and, as will be shown, generates propulsion only within a specific frequency range of flapping. This behaviour contrasts with swimmers in beds of frictional polystyrene spheres (Xiao *et al.* 2025). Both the swimming direction and its frequency dependence differ from those observed in the rigid and frictional particles.

2. Experimental methods and materials

The experimental set-up for the scallop-inspired swimmer in granular media is shown in figure 1 based on our previous study (Xiao *et al.* 2025). The swimmer consists of a pair of counter-rotating, square wings (15 mm × 15 mm, thickness 1 mm), 3D printed from resin. Each wing is mounted on a vertical carbon-fibre rod (diameter 2 mm), supported by ball bearings, with the rods separated by 10 mm. A servo motor drives one rod directly, while the other is coupled through a pair of identical gears, ensuring symmetric counter-rotation of the wings. A Cartesian coordinate system is defined with x the lateral direction, y the swimming direction (figure 1 inset) and z the vertical axis pointing upward. The wings flap between $\theta_1 = 80°$ (opened) and $\theta_2 = 20°$ (closed), respectively.

To prepare the hydrogel granulate, we started from dry powder sieved to a narrow size distribution [0.20, 0.23] mm. After swelling in distilled water, the particles assumed diameters of [1, 2] mm. The hydrogel particles were removed from the water bath with a strainer and placed on paper towels to drain excess surface water. Residual water formed liquid bridges between neighbouring particles, rendering the material slightly cohesive. The liquid bridge-induced cohesion and the deformation behaviours of bulk packing are described in Harth *et al.* (2020), Wang *et al.* (2022) and Farmani *et al.* (2025). The inset of figure 1 shows the bed surface. For comparison, we also used dry polystyrene particles

https://doi.org/10.1017/jfm.2026.11477 Published online by Cambridge University Press

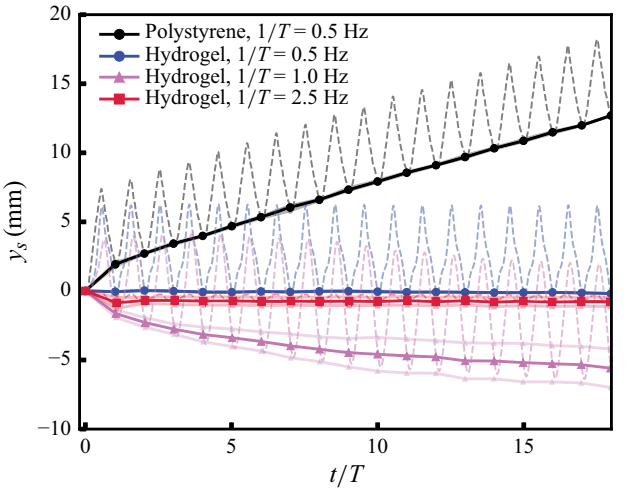


Figure 2. Swimmer displacement as a function of time (dashed curves) for several flapping periods: $T = 2.0$ s (blue), $T = 1.0$ s (purple), $T = 0.4$ s (red). For comparison, the black curve shows data for polystyrene granulate at $T = 2.0$ s. For each case, symbols, connected by solid lines, indicate the displacement at the end of each cycle, averaged over two repetitions, and the corresponding displacement in each repetition is shown as a solid curve with lighter colour.

with an average diameter of 1 mm and a similar density to the hydrogel particles, as examined in greater detail in Xiao *et al.* (2025).

The granulate was contained in a cubic box with a cross-section of 70 mm × 70 mm, filled to a height of 85 mm. The swimmer's mid-xy plane was thus positioned at a depth of 40 mm. The box rested on two linear rails, each supported by two air bearings. The total moving mass was 1.54 kg, including the reservoir and rails. This is far below the load-bearing capacity of the air bearings (4×4.5 kg), allowing frictionless motion in the y direction.

The displacement of the reservoir was recorded by a linear position Hall encoder and converted to the relative displacement of the swimmer, y_s. A load cell measured the force f_y acting on the swimmer in the y direction. Neither the load cell nor the motor was mechanically coupled to the moving granular bed. Swimming was tested in both hydrogel and polystyrene media over a range of cycle periods T, always beginning with the closed angle θ_2.

3. Locomotion in granular media of hydrogel and polystyrene particles

Figure 2 shows the swimmer displacement y_s as a function of scaled time t/T (dashed curves), averaged over two repetitions, with the positive direction (forward) defined in figure 1. In polystyrene granulate, the swimmer exhibits persistent locomotion in the $+y$ direction, consistent with our previous results (Xiao *et al.* 2025). In contrast, locomotion in hydrogel granulate occurs in the $-y$ direction and depends strongly on the flapping rate: at $1/T = 0.5$ Hz, the net displacement vanishes, with the swimmer returning to $y_s = 0$ after each cycle; at $1/T = 1.0$ Hz, the swimmer develops persistent locomotion in the $-y$ direction, opposite to that observed in polystyrene granulate; and at $1/T = 2.5$ Hz, the net displacement has vanished again. For each case, measurements from two individual runs are shown with lighter colours. Results of repeated runs coincide, except for $1/T = 1.0$ Hz, where a slight quantitative difference between the two runs exists. This indicates a slight

https://doi.org/10.1017/jfm.2026.11477 Published online by Cambridge University Press

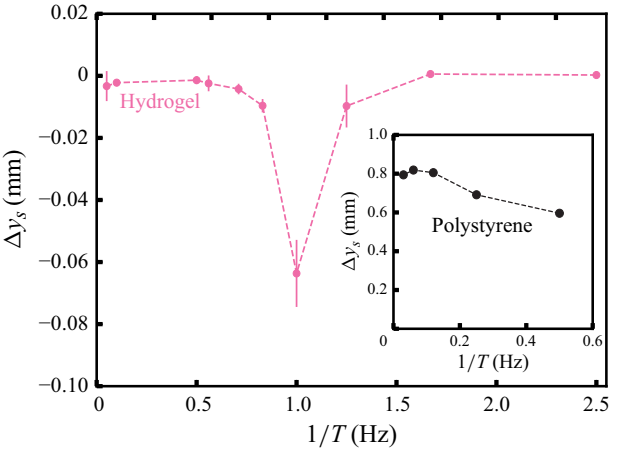


Figure 3. Net swimmer displacement per cycle as a function of the flapping frequency in hydrogel particles. Error bars indicate the differences between two experimental repetitions. The inset shows the data for a swimmer moving in polystyrene particles; here, the error bars are very small.

dependence of the propulsion on the initial packing condition, which may have a stronger history dependence for the cohesive hydrogel granulates than for polystyrene.

Figure 3 shows the net displacement of the swimmer per cycle, Δy_s, as a function of the flapping frequency. These values are averages of the slope of $y_s(t/T)$ at the end of each cycle (symbols in figure 2), quantified by linear fits over at least five successive data points in the linear regime after the initial relaxation ($t/T \geq 5$). We obtain a sharp peak in magnitude at $1/T = 1$ Hz, while for both $1/T \ll 1$ Hz and $1/T \gg 1$ Hz, the motion ceases. For comparison, the inset of figure 3 shows the same data for a swimmer moving in a polystyrene granulate. Although we cannot scan the same frequency range as for hydrogel particles due to limitations of the apparatus, we see that the net displacement per cycle is strictly positive and decreases slightly with increasing frequency $1/T$. This behaviour resembles the rate independence reported for other locomotion problems in plastically deforming granular media (Maladen *et al.* 2009; Hatton *et al.* 2013). Whereas the persistent forward motion in stiff, frictional and non-cohesive granular media is associated with particle jamming in the vicinity of the swimmer (Xiao *et al.* 2025), the backward propulsion observed in hydrogel particles arises from a different mechanism, as discussed below.

While figure 3 presents the average swimmer's net displacement per cycle, figure 4 shows the sub-cycle phase-resolved velocity, $\dot{y}_s(t)$, together with the corresponding driving force, $f_y(t)$, over a period $0 \leqslant t \leqslant T$ for the flapping frequency $1/T = 1$ Hz corresponding to the peak average locomotion velocity. At the start of each stroke, $t/T = \{0, 0.5\}$, the swimmer initially continues to move in the direction set by the preceding stroke, despite the reversal of the motion of the wings. During this period, the work done by the driving force is negative ($\dot{y}_s f_y < 0$), which decelerates the swimmer over a duration $\Delta t/T \approx 0.1$, until $|\dot{y}_s| = 0$. This behaviour suggests that the swimmer's inertia cannot be neglected. If inertia were negligible, the swimmer would instantly follow the direction of wing motion and its velocity would change sign immediately at $t/T = \{0, 0.5\}$.

The swimming motion observed in our experiment occurs when the space-fixed swimmer moves relative to the frictionless container filled with hydrogel granulate. The effective mass associated with this motion is, therefore, that of the container and the hydrogel granulate, rather than the mass of the swimmer itself. Consequently, our

https://doi.org/10.1017/jfm.2026.11477 Published online by Cambridge University Press

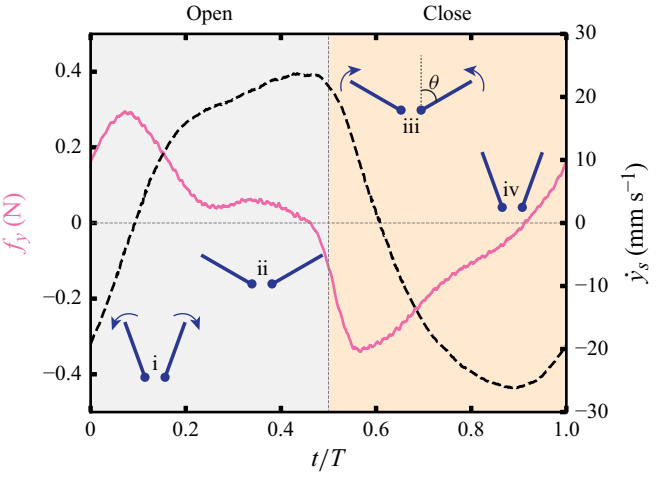


Figure 4. Phase-resolved swimmer velocity (black dashed line, right axis) and driving force (red solid line, left axis) at a flapping frequency of $1/T = 1$ Hz in hydrogel particles. The vertical dotted line separates the opening and closing half-cycles, sketched in the insets.

experimental set-up corresponds to a free swimmer (neglecting rotation) whose density exceeds that of the ambient fluid by orders of magnitude. The high density should only affect the swimmer's inertia, not its buoyancy. Therefore, a free-swimmer experiment that corresponds to our fixed-swimmer set-up should be carried out in the absence of gravity.

A closely related system was investigated by Gonzalez-Rodriguez & Lauga (2009) and Hubert *et al.* (2021), who found that reciprocal swimming is possible in a Newtonian fluid within the Stokes regime, provided the swimmer's density is much larger than that of the fluid, $\rho_s \gg \rho_f$. In this case, the swimmer-based Reynolds number, $Re_s = \rho_s L^2/(T\eta)$, is finite, whereas the Reynolds number of the fluid, $Re_f = \rho_f L^2/(T\eta)$, is negligible. Here, L denotes the characteristic length of the swimmer and η the viscosity of the fluid. The analytical result by Gonzalez-Rodriguez & Lauga (2009) then predicts a cycle-averaged net velocity in the $-y$ direction that increases with the flapping frequency, $1/T$.

Although we acknowledge the substantial differences between the system examined by Gonzalez-Rodriguez & Lauga (2009) and our own, we note that the direction of motion (along $-y$) and the frequency dependence are similar, at least for low frequencies up to $1/T \approx 1$ Hz, cf. figure 3. At higher frequencies, however, the viscoelastic properties of the hydrogel become significant, and local density variations within the granulate arise due to the rapid motion of the wings. These effects will be discussed in detail in the following sections.

4. Dynamics of swimming in hydrogels

4.1. *Inertia*

The dynamics of the system is determined by the accelerated mass, the flapping period T and the viscoelastic properties of the granulate, which relate the swimmer to the granulate-filled container. In our experiment, the swimmer is fixed in space, therefore, the relevant mass is the mass of the movable granulate-filled container. For a very low frequency, $1/T = 0.05$ Hz, the container follows the flapping wings approximately, with no noticeable net displacement over one period, as evidenced by a symmetric displacement profile for the opening and closing half-periods, see figure 5. The phase-resolved

https://doi.org/10.1017/jfm.2026.11477 Published online by Cambridge University Press

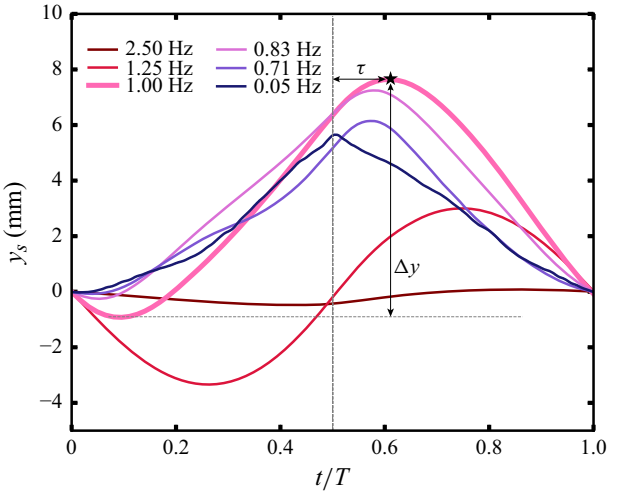


Figure 5. Averaged relative displacement of the swimmer as a function of the phase, t/T, for various flapping frequencies in hydrogel particles. For each case, the average was taken over at least five individual cycles beyond the initial transients. The vertical dotted line separates the opening and closing half-cycles. The figure also defines the (positive) peak location, τ, and the peak-to-peak amplitude, Δy, that depend on the flapping frequency, see figure 6.

displacement was obtained by averaging over all periods, disregarding the initial transient. Note that the net transport per cycle, shown in figure 2, is much smaller than the typical peak displacement. With its accelerated mass and the restoring force from the granulate, the container may thus be regarded as a driven nonlinear oscillator, oscillating about the swimmer's position with a superimposed slow drift. For slow flapping, $1/T = 0.05$ Hz, the force acting on the container is small, and the container follows the driving flaps without appreciable deformation of the granular particles. Consequently, the trajectory $y_s(t/T)$ is symmetric between the two half-cycles. For fast flapping ($1/T = 2.5$ Hz), the container cannot follow the driving motion owing to its inertia. The wings strongly deform the granular particles, but their low elastic modulus prevents sufficient force transfer to accelerate the container appreciably, thus, $\Delta y \to 0$.

The inertia-based mechanism described above introduces a phase shift τ between the wing actuation and the relative displacement of the swimmer and container. While the phase shift τ increases with flapping frequency, the amplitude of the induced oscillation, Δy (defined in figure 5), varies non-monotonically. In the limit $1/T \to 0$, the container follows the driving motion and Δy approaches a constant value, $\Delta y^{(0)}$. In the opposite limit $T \to 0$, $\Delta y \to 0$ owing to the low elastic modulus of the medium. At intermediate frequency, $1/T$, we observe amplitudes $\Delta y(T) > \Delta y^{(0)}$, resembling resonant oscillations.

This analysis is supported by figure 6, which shows the phase shift $2\pi\tau$ and the peak-to-peak amplitude Δy as functions of the flapping frequency $1/T$. The dotted lines reveal that the frequency at which Δy reaches its maximum coincides with the frequency of fastest locomotion, while the phase shift experiences a rapid increase from $2\pi\tau \approx \pi/4$ to $2\pi\tau \approx \pi/2$. These trends in Δy and τ resemble those of a periodically driven damped oscillator, with resonance occurring near 1 Hz, which is the frequency of maximum locomotion velocity plotted in figure 3.

To clarify this coincidence, we examine the nature of the forces exerted on the swimmer by the hydrogel medium.

https://doi.org/10.1017/jfm.2026.11477 Published online by Cambridge University Press

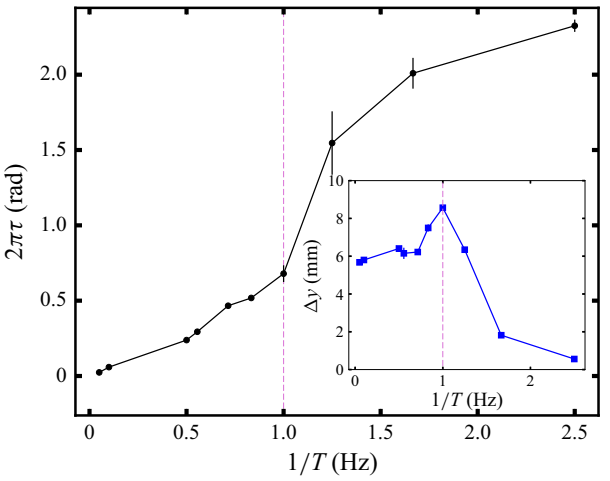


Figure 6. Phase shift τ and peak-to-peak amplitude Δy (inset) as functions of the flapping frequency in hydrogel particles. The vertical dashed lines mark the frequency of maximal locomotion (see figure 2). Error bars indicate the differences between two experimental repetitions, which are very small for Δy. The standard errors (not shown) in the cycle-averaged $2\pi\tau$ and Δy are also negligible. Lines guide the eye.

4.2. *Viscoelastic relaxation in the hydrogel*

Depending on the deformation rate, hydrogels exhibit both viscous and elastic behaviours. The hydrogel's response determines the interaction force and thus the swimmer's dynamics. We examined the viscoelastic response in relaxation experiments. In case (*a*), with the air bearings blocked to prevent reservoir displacement, the swimmer's wings were rapidly opened from $\theta = 20°$ to $\theta = 80°$ at $t = 0$, and the subsequent relaxation of the force (magnitude) on the swimmer, F_y, was recorded. Case (*b*) was analogous, except that the wings were rapidly closed from $\theta = 80°$ to $\theta = 20°$ at $t = 0$.

Figure 7 shows the measured forces, which exhibit a rapid decay within the first few seconds followed by a slower relaxation toward a long-term residual value, reflecting the combined viscous and elastic response of the medium.

We fitted the function

$$F_y = \alpha \left(e^{-t/\tau_1} + e^{-t/\tau_2}\right) + F_\infty, \tag{4.1}$$

to the measured forces over $t \in [0, 20]$ s to obtain the relaxation times: τ_1 possibly associated with the responses at the individual particle level, including the dissipation within the hydrogel material and the inter-particle capillary bridges (Farmani *et al.* 2025), and τ_2, associated with particle rearrangements, with $\tau_1 < \tau_2$. Averaging over opening and closing strokes gives $\tau_1 \approx 0.3$ s and $\tau_2 \approx 4.9$ s. Remarkably, the peak in backward locomotion at 1 Hz (see figure 2) lies between $1/\tau_1 \approx 3.3$ Hz and $1/\tau_2 \approx 0.2$ Hz. The corresponding Deborah numbers, $De_{\{1,2\}} = \tau_{\{1,2\}}/T$, are of the order of unity, indicating that both elastic and viscous effects contribute significantly to the swimmer's propulsive force. Further increasing the swimming frequency may result in enhanced elastic effects. The corresponding decrease in the swimmer's net displacement may be similar to that observed in Keim *et al.* (2012), where the propulsion speed of an oscillating dumbbell in a viscoelastic fluid reaches a peak at $De \approx 4$. Note that the residual force F_∞ also contributes to the initial force. On the experimental time scale, $T < 20$ s, it is effectively elastic.

https://doi.org/10.1017/jfm.2026.11477 Published online by Cambridge University Press

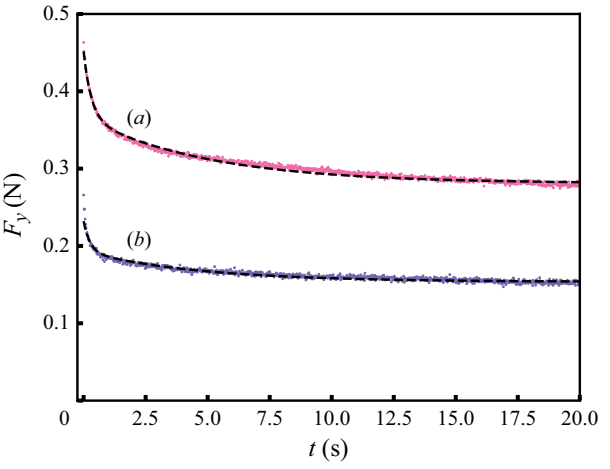


Figure 7. Relaxation of the swimming force following a rapid stroke in hydrogel particles. For opening (*a*), the data are fitted to (4.1) (dashed curve) with $\alpha = 0.085$ N, $\tau_1 = 0.31$ s, $\tau_2 = 5.02$ s and $F_\infty = 0.281$ N. For closing (*b*), we obtain $\alpha = 0.039$ N, $\tau_1 = 0.26$ s, $\tau_2 = 4.72$ s and $F_\infty = 0.154$ N.

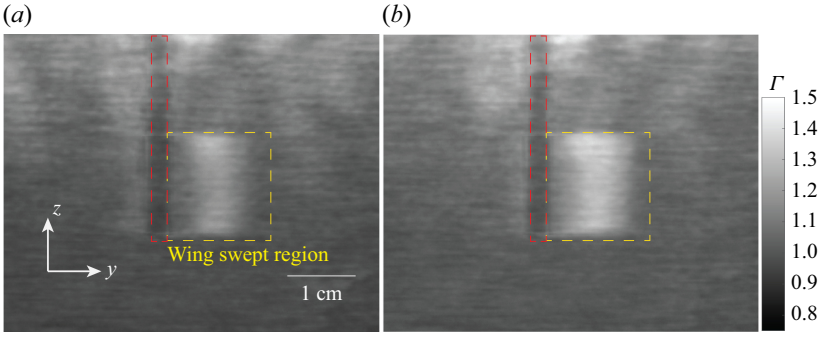


Figure 8. Time-averaged X-ray radiographs of the swimmer flapping with frequency $1/T = 0.05$ Hz (*a*) and $1/T = 1$ Hz (*b*) in hydrogel particles. In each case, the average was taken over entire swimming cycles for at least five cycles. Yellow boxes mark the regions swept by the wings, and red boxes indicate the position of the mounting rod. A higher intensity Γ corresponds to a lower density in the hydrogel medium.

4.3. *Variation of density in hydrogel media*

Rearrangement of the hydrogel particles, characterised by the relaxation time τ_2, occurs on a slower time scale than the wing motion, leading to densification of the medium in front of the moving wing and dilatation behind it. Whereas densification is limited by the material density of the hydrogel particles, dilatation is not, since air-filled voids may form between the granular particles. Consequently, the average density of the hydrogel granular medium over a flapping period is smaller in the volume swept by the wings than in regions far from the wings. Particle reordering counteracts this effect. Therefore, the difference in density is more pronounced for faster flapping, evidenced by figure 8, showing X-ray radiographs of the swimmer and the hydrogel granulate in the yz plane (see figure 1). The radiographs (110 kV, 400 μA) were recorded at 10 fps and averaged over all frames acquired during at least five flapping cycles.

Comparison of the X-ray images in panels (*a*) and (*b*) shows that the granulate density in the region swept by the wings (yellow box) is lower during fast flapping ($1/T = 1$ Hz)

https://doi.org/10.1017/jfm.2026.11477 Published online by Cambridge University Press

than during slow flapping ($1/T = 0.05$ Hz). (Because of speed limitations in the X-ray imaging, radiographs could not be obtained for faster wing rotations.) Thus, owing to the relaxation time τ_2, voids form in the vicinity of the wings due to the viscoelasticity of the hydrogel granulate. For $T \sim \tau_2$, the voids can be at least partially refilled during each stroke by particle rearrangements, leading to hysteresis in the swimming cycle despite the reciprocal wing motion. For $T \ll \tau_2$, particle reordering cannot keep pace with the wing motion, therefore voids persist during both opening and closing strokes, and symmetry remains unbroken. This is reminiscent of the propulsion loss observed in bacteria moving through dense polymer solutions, where a nanometre-sized flagellum is believed to deplete nearby polymer coils (Martinez *et al.* 2014). In our study, the use of air as the interstitial fluid provides high contrast against the particles, enabling direct X-ray visualisation of this non-continuum effect.

4.4. *Implications for locomotion*

From the examination of inertial and viscoelastic effects in §§ 4.1, 4.2 and 4.3, a consistent picture emerges for the propagation of a swimmer in a hydrogel granular medium, as shown in figure 2. To support the subsequent discussion, we introduce an idealised dynamical equation for the swimmer. Although the precise mathematical form of each term is not guaranteed, the equation should at least capture the essential features of the dynamics

$$m\frac{d^2y_s}{\mathrm{d}t^2} + \gamma(\theta)\frac{\mathrm{d}y_s}{\mathrm{d}t} + \kappa(\theta)(y_s - y_0(t)) = f_{wing}(\theta). \tag{4.2}$$

Here, m is the mass of the movable container, γ is the drag coefficient, κ an elastic constant and f_{wing} the driving force generated by the wing's motion. All terms depend on the instantaneous wing angle θ. In addition, the coefficients γ and κ, as well as the driving force f_{wing}, depend on the density of the granular medium in a complex manner that is not addressed here. In the stationary state, the mean position y_0 drifts at the rate $\Delta y_s/T$, as plotted in figure 3. We now discuss the system in three characteristic flapping regimes:

(i) For $1/T \gg 1$ Hz viscous effects cease as $T \ll \tau_1 < \tau_2$. Here, $\gamma \approx 0$, so the swimmer effectively flaps in an elastic medium while generating long-lasting voids. Owing to the absence of relaxation, $y_0(t) \approx 0$, and (4.2) therefore describes harmonic oscillations without locomotion.

(ii) For $1/T \ll 1$ Hz, inertia does not influence swimming, as evidenced by the negligible phase shift in figure 6. In this regime, the inertial term $m\,d^2y_s/\mathrm{d}t^2$ is obsolete, and (4.2) depends only on the wing angle θ. At very low frequencies, particle rearrangements in the hydrogel granulate are fast enough to refill the voids during each stroke, making (4.2) effectively density independent. This situation resembles the original scallop theorem, which prohibits locomotion despite strong elastic effects, as seen in figure 7.

(iii) For $1/T \approx 1$ Hz, viscous and elastic effects coexist, and inertia becomes significant. In this regime, all terms in (4.2) contribute, with the microscopic origin linked to hysteresis in the granular density caused by partial refilling of voids on the time scale $\tau_2 \sim T$. While the interplay between inertia and viscous effects results in the net swimmer displacement per cycle, it is likely that the interplay between elastic and inertial effects amplifies the net displacement magnitude via a behaviour that resembles resonance, as shown in figure 6. This facilitates the energy transfer between the swimmer and the medium due to the phase shift (figures 4 and 6),

https://doi.org/10.1017/jfm.2026.11477 Published online by Cambridge University Press

allowing $\gamma \mathrm{d}y_s/\mathrm{d}t$ and f_{wing} to act in the same direction after a switch of the wing rotation direction. This eventually results in a maximum net swimmer displacement at $1/T \approx 1$ Hz.

5. Summary

In summary, a scallop-like swimmer with reciprocally flapping wings in a granular bed of hydrogel spheres can achieve backward locomotion within a certain range of flapping frequencies. This behaviour arises from the combined effects of inertia and viscoelasticity of the soft granular hydrogel medium. The locomotion and its underlying mechanisms differ fundamentally from previous observations in idealised rigid granular media, such as plastic beads (Xiao *et al.* 2025).

Acknowledgements. R.S. and J.W. acknowledge funding by DLR within project 50WK2348. The authors would like to thank A. Nazemi for fruitful discussions.

Declaration of interests. The authors report no conflicts of interest.

Author contributions. H.X. and J.W. have contributed equally to this work.

References

AGARWAL, S., GOLDMAN, D.I. & KAMRIN, K. 2023 Mechanistic framework for reduced-order models in soft materials: application to three-dimensional granular intrusion. *Proc. Natl Acad. Sci. USA* **120** (4), e2214017120.

AGARWAL, S., KARSAI, A., GOLDMAN, D.I. & KAMRIN, K. 2021 Surprising simplicity in the modeling of dynamic granular intrusion. *Sci. Adv.* **7** (17), eabe0631.

ARRATIA, P.E. 2022 Life in complex fluids: swimming in polymers. *Phys. Rev. Fluids* **7** (11), 110515.

ASHOUR, A., TRITTEL, T., BÖRZSÖNYI, T. & STANNARIUS, R. 2017 Silo outflow of soft frictionless spheres. *Phys. Rev. Fluids* **2**, 123302.

ASKARI, H. & KAMRIN, K. 2016 Intrusion rheology in grains and other flowable materials. *Nat. Mat.* **15** (12), 1274–1279.

BALIN, A.K., ZÖTTL, A., YEOMANS, J.M. & SHENDRUK, T.N. 2017 Biopolymer dynamics driven by helical flagella. *Phys. Rev. Fluids* **2** (11), 113102.

BEHRINGER, R.P. & CHAKRABORTY, B. 2018 The physics of jamming for granular materials: a review. *Rep. Prog. Phys.* **82** (1), 012601.

BI, D., ZHANG, J., CHAKRABORTY, B. & BEHRINGER, R.P. 2011 Jamming by shear. *Nature* **480** (7377), 355–358.

BINAGIA, J.P. & SHAQFEH, E.S.G. 2021 Self-propulsion of a freely suspended swimmer by a swirling tail in a viscoelastic fluid. *Phys. Rev. Fluids* **6** (5), 053301.

BRZINSKI III, T.A., MAYOR, P. & DURIAN, D.J. 2013 Depth-dependent resistance of granular media to vertical penetration. *Phys. Rev. Lett.* **111** (16), 168002.

BUCHHOLTZ, V. & PÖSCHEL, T. 1998 Interaction of a granular stream with an obstacle. *Granul. Matt.* **1**, 33–41.

DATTA, S.S. et al. 2022 Perspectives on viscoelastic flow instabilities and elastic turbulence. *Phys. Rev. Fluids* **7** (8), 080701.

DIJKSMAN, J.A. & MULLIN, T. 2022 Creep control in soft particle packings. *Phys. Rev. Lett.* **128**, 238002.

DORGAN, K.M. 2018 Kinematics of burrowing by peristalsis in granular sands. *J. Expl Biol.* **221** (10), jeb167759.

FARMANI, Z., WANG, J., STANNARIUS, R. & DIJKSMAN, J. 2025 Capillary-induced adhesive contact dynamics determines dissipation and flow structure in wetted hydrogel packings. *Soft Matt.* **21**, 5468–5479.

FORTERRE, Y. & POULIQUEN, O. 2008 Flows of dense granular media. *Annu. Rev. Fluid Mech.* **40** (1), 1–24.

FU, H.C., SHENOY, V.B. & POWERS, T.R. 2010 Low-Reynolds-number swimming in gels. *Europhys. Lett.* **91** (2), 24002.

FU, H.C., WOLGEMUTH, C.W. & POWERS, T.R. 2009 Swimming speeds of filaments in nonlinearly viscoelastic fluids. *Phys. Fluids* **21**, 033102.

GOLDMAN, D.I. 2014 Colloquium: biophysical principles of undulatory self-propulsion in granular media. *Rev. Mod. Phys.* **86** (3), 943–958.

https://doi.org/10.1017/jfm.2026.11477 Published online by Cambridge University Press

GONZALEZ-RODRIGUEZ, D. & LAUGA, E. 2009 Reciprocal locomotion of dense swimmers in Stokes flow. *J. Phys.: Condens. Matter* **21** (20), 204103.
HAN, K., SHIELDS IV, C.W., BHARTI, B., ARRATIA, P.E. & VELEV, O.D. 2020 Active reversible swimming of magnetically assembled 'microscallops' in non-Newtonian fluids. *Langmuir* **36** (25), 7148–7154.
HARRINGTON, M., XIAO, H. & DURIAN, D.J. 2020 Stagnant zone formation in a 2D bed of circular and elongated grains under penetration. *Granul. Matt.* **22**, 17.
HARTH, K., WANG, J., BÖRZSÖNYI, T. & STANNARIUS, R. 2020 Intermittent flow and transient congestions of soft spheres passing narrow orifices. *Soft Matt.* **16** (34), 8013–8023.
HATTON, R.L., DING, Y., CHOSET, H. & GOLDMAN, D.I. 2013 Geometric visualization of self-propulsion in a complex medium. *Phy. Rev. Lett.* **110** (7), 078101.
HUBERT, M., TROSMAN, O., COLLARD, Y., SUKHOV, A., HARTING, J., VANDEWALLE, N. & SMITH, A.-S. 2021 Scallop theorem and swimming at the mesoscale. *Phys. Rev. Lett.* **126** (22), 224501.
KANG, W., FENG, Y., LIU, C. & BLUMENFELD, R. 2018 Archimedes' law explains penetration of solids into granular media. *Nat. Commun.* **9** (1), 1101.
KEIM, N.C., GARCIA, M. & ARRATIA, P.E. 2012 Fluid elasticity can enable propulsion at low Reynolds number. *Phys. Fluids* **24** (8), 081703.
KROO, L.A., BINAGIA, J.P., ECKMAN, N., PRAKASH, M. & SHAQFEH, E.S.G. 2022 A freely suspended robotic swimmer propelled by viscoelastic normal stresses. *J. Fluid Mech.* **944**, A20.
LAUGA, E. 2011 Life around the scallop theorem. *Soft Matt.* **7** (7), 3060–3065.
LIU, A.J. & NAGEL, S.R. 1998 Jamming is not just cool any more. *Nature* **396** (6706), 21–22.
MAJMUDAR, T.S., SPERL, M., LUDING, S. & BEHRINGER, R.P. 2007 Jamming transition in granular systems. *Phys. Rev. Lett.* **98** (5), 058001.
MALADEN, R.D., DING, Y., LI, C. & GOLDMAN, D.I. 2009 Undulatory swimming in sand: subsurface locomotion of the sandfish lizard. *Science* **325** (5938), 314–318.
MARTINEZ, V.A., SCHWARZ-LINEK, J., REUFER, M., WILSON, L.G., MOROZOV, A.N. & POON, W.C.K. 2014 Flagellated bacterial motility in polymer solutions. *Proc. Natl Acad. Sci. USA* **111** (50), 17771–17776.
MONTANA, J., FINN, J.K. & NORMAN, M.D. 2015 Liquid sand burrowing and mucus utilisation as novel adaptations to a structurally-simple environment in Octopus kaurna Stranks, 1990. *Behaviour* **152** (14), 1871–1881.
MÜLLER, P., FORMELLA, A. & PÖSCHEL, T. 2014 Granular jet impact: probing the ideal fluid description. *J. Fluid Mech.* **751**, 601–626.
NORMAND, T. & LAUGA, E. 2008 Flapping motion and force generation in a viscoelastic fluid. *Phys. Rev. E* **78** (6), 061907.
PAK, O.S., ZHU, L., BRANDT, L. & LAUGA, E. 2012 Micropropulsion and microrheology in complex fluids via symmetry breaking. *Phys. Fluids* **24** (10), 103102.
PURCELL, E.M. 1977 Life at low Reynolds number. *Am. J. Phys.* **45** (1), 3–11.
QIU, T., LEE, T.-C., MARK, A.G., MOROZOV, K.I., MÜNSTER, R., MIERKA, O., TUREK, S., LESHANSKY, A.M. & FISCHER, P. 2014 Swimming by reciprocal motion at low Reynolds number. *Nat. Commun.* **5** (1), 1–8.
RILEY, E.E. & LAUGA, E. 2017 Empirical resistive-force theory for slender biological filaments in shear-thinning fluids. *Phys. Rev. E* **95** (6), 062416.
ROGOWSKI, L.W., ALI, J., ZHANG, X., WILKING, J.N., FU, H.C. & KIM, M.J. 2021 Symmetry breaking propulsion of magnetic microspheres in nonlinearly viscoelastic fluids. *Nat. Commun.* **12** (1), 1116.
SCHALL, P. & VAN HECKE, M. 2010 Shear bands in matter with granularity. *Annu. Rev. Fluid Mech.* **42**, 67–88.
SHAKYA, C., VAN DER GUCHT, J. & DIJKSMAN, J.A. 2024 Viscoelastic material properties determine the contact mechanics of hydrogel spheres. *Frontiers Phys.* **12**, 1334325.
STANNARIUS, R., MARTINEZ, D.S., BÖRZSÖNYI, T., BIEBERLE, M., BARTHEL, F. & HAMPEL, U. 2019 High-speed x-ray tomography of silo discharge. *New J. Phys.* **21**, 113054.
WANG, J., FAN, B., PONGÓ, T., BÖRZSÖNYI, T., HIDALGO, R.C. & STANNARIUS, R. 2023 Force on a sphere suspended in flowing granulate. *Phys. Rev. E* **108** (6), L062901.
WANG, J., FARMANI, Z., DIJKSMAN, J.A., LÜBECK, C., SPECK, O. & STANNARIUS, R. 2022 Characterization of shear zones in soft granular beds by means of a novel magnetic resonance imaging technique. *Granul. Matt.* **24** (4), 103.
WRÓBEL, J.K., LYNCH, S., BARRETT, A., FAUCI, L. & CORTEZ, R. 2016 Enhanced flagellar swimming through a compliant viscoelastic network in Stokes flow. *J. Fluid Mech.* **792**, 775–797.
XIAO, H., HRUSKA, J., OTTINO, J.M., LUEPTOW, R.M. & UMBANHOWAR, P.B. 2018 Unsteady flows and inhomogeneous packing in damp granular heap flows. *Phys. Rev. E* **98** (3), 032906.

https://doi.org/10.1017/jfm.2026.11477 Published online by Cambridge University Press

XIAO, H., IVANCIC, R.J.S. & DURIAN, D.J. 2020 Strain localization and failure of disordered particle rafts with tunable ductility during tensile deformation. *Soft Matt.* **16** (35), 8226–8236.

XIAO, H., OTTINO, J.M., LUEPTOW, R.M. & UMBANHOWAR, P.B. 2017 Transient response in granular quasi-two-dimensional bounded heap flow. *Phys. Rev. E* **96** (4), 040902.

XIAO, H., TORRES, H., SACK, A. & PÖSCHEL, T. 2025 Locomotion of a scallop-inspired swimmer in granular matter. *Phys. Rev. Appl.* **24** (3), 034049.

XIAO, H., ZHANG, G., YANG, E., IVANCIC, R., RIDOUT, S., RIGGLEMAN, R., DURIAN, D.J. & LIU, A.J. 2023 Identifying microscopic factors that influence ductility in disordered solids. *Proc. Natl Acad. Sci. USA* **120** (42), e2307552120.

ZHANG, Y., LI, G. & ARDEKANI, A.M. 2018 Reduced viscosity for flagella moving in a solution of long polymer chains. *Phys. Rev. Fluids* **3** (2), 023101.

https://doi.org/10.1017/jfm.2026.11477 Published online by Cambridge University Press